

## VIP Cross-Coupling Very Important Paper

How to cite: *Angew. Chem. Int. Ed.* **2023**, 62, e202218775

International Edition: doi.org/10.1002/anie.202218775

German Edition: doi.org/10.1002/ange.202218775

# Enforced Electronic-Donor-Acceptor Complex Formation in Water for Photochemical Cross-Coupling

Ya-Ming Tian, Evamaria Hofmann, Wagner Silva, Xiang Pu, Didier Touraud, Ruth M. Gschwind, Werner Kunz, and Burkhard König\*

**Abstract:** The amino alcohol meglumine solubilizes organic compounds in water and enforces the formation of electron donor acceptor (EDA) complexes of haloarenes with indoles, anilines, anisoles or thiols, which are not observed in organic solvents. UV-A photoinduced electron transfer within the EDA complexes induces the mesolytic cleavage of the halide ion and radical recombination of the arenes leading, after rearomatization and proton loss to C–C or C–S coupling products. Depending on the substitution pattern selective and unique cross-couplings are observed. UV and NMR measurements reveal the importance of the assembly for the photoinduced reaction. Enforced EDA aggregate formation in water allows new activation modes for organic photochemical synthesis.

## Introduction

The aggregation of an electron-donating molecule with low ionization potential and an electron-accepting compound with high electron affinity in the ground state can result in the formation of an Electron Donor-Acceptor (EDA) complex.<sup>[1]</sup> Electronic coupling from the frontier orbitals of the two independent molecules induce different physical properties of the EDA complex from those of the interacting molecules.<sup>[2]</sup> EDA complexes typically exhibit new absorption bands at longer wavelengths which provide the possibility to activate the substrates by visible light irradiation without the presence of sensitizers or photoredox catalysts.<sup>[2–5]</sup> Although investigations of the photophysical

properties of EDA complexes date back to the 1950s,<sup>[1,2,6–10]</sup> their application in photochemical synthesis started much later. In the 1970s, pioneering, but rather narrow, studies demonstrated that EDA complexes can be chemically transformed via radical processes under light irradiation,<sup>[11–18]</sup> but only from 2013 on, EDA photochemistry was wider recognized and applied as an independent strategy for radical chemistry in synthesis.<sup>[5,19–36]</sup> Synthetic applications driven by the photoactivity of EDA complexes now embrace many compound classes and bond formations, including many stereoselective transformations. Recent reviews summarize the state of the field very well.<sup>[4,5]</sup>

The association in EDA complexes is not as directional and robust as other interactions, e.g., hydrogen bonding, and the strength of electron donor-acceptor association is sensitive to various factors, such as solvent, temperature and concentration.<sup>[3–5]</sup> In addition, the formation of EDA complexes and the selectivity of their subsequent transformations can be affected by their local environment, which has been used in asymmetric enzyme photocatalysis.<sup>[5,37–39]</sup> Electron-rich cofactors as electron donors can form EDA complexes with electron-deficient molecules, facilitated by close proximity in the active site of the enzyme. Such enzyme stabilized charge transfer complexes subsequently generate radical intermediates upon irradiation, which remain in the position of the active site. The chiral environment within the enzyme induces product stereoselectivity, and with the release of the product from the active site, the photo- and enzyme-catalyzed process starts again. Recent examples from the Hyster group include the light-induced dehalogenation of racemic halolactones to chiral lactones in the active site of ketoreductases<sup>[38]</sup> and the biocatalytic cyclization of  $\alpha$ -chloroamides by photoexcitation of flavoenzymes.<sup>[39]</sup>

Solvent effects have great potential to act as an external force affecting the photochemical properties of EDA complexes, since it has been reported that the nature of the solvent not only plays a crucial role in the formation and stability of EDA complexes, but also affects the electron transfer process.<sup>[3,4]</sup> Excitation of the EDA complex and the electron transfer process are accompanied by solvent reorientation, especially in polar solvents.<sup>[3,4]</sup> In addition, the excited state species are more polarized than their ground states, resulting in stronger solvation in polar solvents which positively affects relaxation dynamics of reactive intermediates.<sup>[3,4]</sup> Water as the most polar medium among common solvents, is expected to affect properties and transformations of EDA complexes. However, to the best of

[\*] Dr. Y.-M. Tian, Dr. W. Silva, X. Pu, Prof. Dr. R. M. Gschwind, Prof. Dr. B. König  
 Faculty of Chemistry and Pharmacy, Institute of Organic Chemistry, University Regensburg  
 93040 Regensburg (Germany)  
 E-mail: burkhard.koenig@chemie.uni-regensburg.de  
 E. Hofmann, Dr. D. Touraud, Prof. Dr. W. Kunz  
 Faculty of Chemistry and Pharmacy, Institute of Physical and Theoretical Chemistry, University Regensburg  
 93040 Regensburg (Germany)

© 2023 The Authors. Angewandte Chemie International Edition published by Wiley-VCH GmbH. This is an open access article under the terms of the Creative Commons Attribution License, which permits use, distribution and reproduction in any medium, provided the original work is properly cited.

our knowledge, the synthetic use of EDA complexes in water has not been investigated in detail, likely due to the low solubility of most organic compounds in water and sensitivity to hydrolysis of functional groups or intermediates.

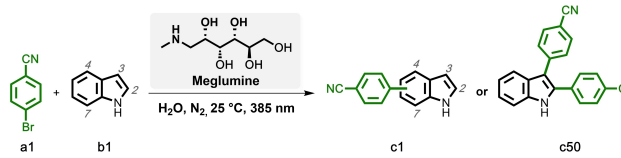
Meglumine is a sugar alcohol containing five hydroxyl groups and one secondary amino group, derived from sorbitol.<sup>[40,41]</sup> The compound is an FDA-approved pharmaceutical excipient.<sup>[41]</sup> In addition to its low cost, high solubility in water, low toxicity, non-corrosiveness, biocompatibility and biodegradability,<sup>[40,41]</sup> it is used in organic synthesis as hydrogen bond or electron donor.<sup>[40–46]</sup> In particular, meglumine has been shown to significantly improve the solubility and stability of poorly water-soluble compounds in water.<sup>[40,42–45,47]</sup>

The formation of light-absorbing enforced EDA complexes from aryl halides and indoles, anilines, anisoles, or thiols has been observed, when dissolved in water. Key to the method is the addition of the amino-sugar alcohol meglumine. This compound enhances the water solubility of organic aromatic compounds to synthetically useful levels, which is essential for effective EDA complex formation. Using meglumine solubilizing properties, radical arylation and arylthiolation of (hetero)aryl halides in water as reaction medium under 385 nm light irradiation has been developed (Figure 1). The conditions allow direct C–H arylation of the benzene ring of indoles, a transformation which has not been observed in EDA photochemistry in organic solvents.

## Results and Discussion

We started our investigation by employing 4-bromobenzonitrile (**a1**) as electron acceptor, indole (**b1**) as electron donor and water as solvent. At first, a range of commercially available polyhydroxy additives was screened, with meglumine proving to be optimal (Table S1), giving a mixture of C2- and C7-arylated products (C2:C7=1:1) in 83 % yield (Table 1, entry 1) at 25 °C under 385 nm light irradiation. Other similar amino-sugar alcohols (Table S1, entries 2, 3, 6, 7) were also capable of promoting the reaction to varying degrees, although providing lower yields. No or trace products were detected in commonly used organic solvents (Table S2), proving the positive effect of water on this reaction. Light sources at longer wavelength resulted in

**Table 1:** Control experiments for the reaction of 4-bromobenzonitrile with indole.



Entry	Deviations from Optimized Conditions	Yields <sup>[a]</sup>	
		c1 (C2:C7)	c50
1	None	83 % (1:1)	n.d.
2	No meglumine	34 % (1:1)	n.d.
3	No light, 25 °C	n.d.	n.d.
4	No light, 60 °C	n.d.	n.d.
5	No light, 90 °C	n.d.	n.d.
6 <sup>b</sup>	60 °C instead of 25 °C	82 % (1:1)	5 %
7	2 °C instead of 25 °C	27 % (1.3:1)	n.d.
8	0.7 W LED	73 % (1:1)	n.d.
9	<b>a1</b> (0.4 mmol), <b>b1</b> (0.1 mmol), meglumine (0.4 mmol), 80 °C	15 % (1:1)	72 %

Standard reaction conditions: **a1** (0.1 mmol), **b1** (0.15 mmol) and meglumine (0.25 mmol) in 2 mL H<sub>2</sub>O under 385 nm LED (2.4 W) light irradiation at 25 °C under N<sub>2</sub> atmosphere for 15 h. n.d., product was not detected. [a] Yields were determined by GC-MS analysis with n-dodecane as an internal standard and are the average of two runs. [b] Reaction time: 12 h.

lower yields, and 365 nm light source was found to be similarly effective (Table S3). The conversion of 4-bromobenzonitrile is influenced by the amount of indole and meglumine, with 1.5 equivalents of indole and 2.5 equivalents of meglumine providing the best conversion (Tables S4 and S5). The reaction gave much lower yield in the absence of the additive (Table 1, entry 2), indicating the crucial role of meglumine. In the dark, no product was detected at 25 °C or higher temperatures (Table 1, entries 3–5), ruling out a thermal pathway. The adjustment of temperature did not greatly affect the selectivity of the products, but the high temperature accelerated the reaction (Table 1, entries 6 and 7). A light source with lower power decreased the product yield (Table 1, entry 8). 72 % of the bis-arylation product **c50** was detected (Table 1, entry 9) when **a1** and meglumine were adjusted to 4 times the equivalent of **b1** and the temperature was raised to 80 °C (see Supporting Information Table S6 for details).

With the optimized conditions in hand, we further examined the scope of this method (Scheme 1 and 2). Under optimal conditions for monoarylation, indoles substituted with methyl (**c2**, **c3**) or methoxy (**c4**) groups on the benzene ring underwent C–H arylation at C2 and C7 positions, giving a mixture in a nearly 1:1 ratio. 6-aminoindole showed high selectivity at the C7 position (**c5–c9**), which may be explained by tighter  $\pi$ - $\pi$  interaction between arene rings of the two reactants due to the electron-donating NH<sub>2</sub> group locating the EDA complex<sup>[3,4]</sup> rather than the benzene part than the pyrrole ring of indole. In addition, the excited EDA complex formed from local band irradiation is dynamically assembled and therefore requires solvent

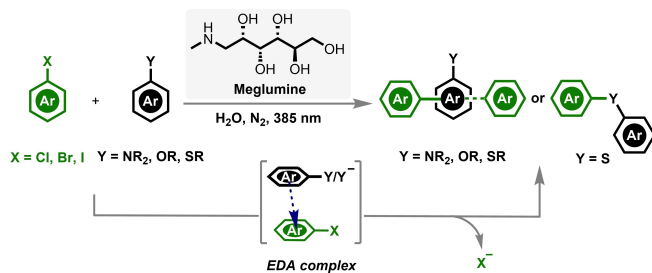
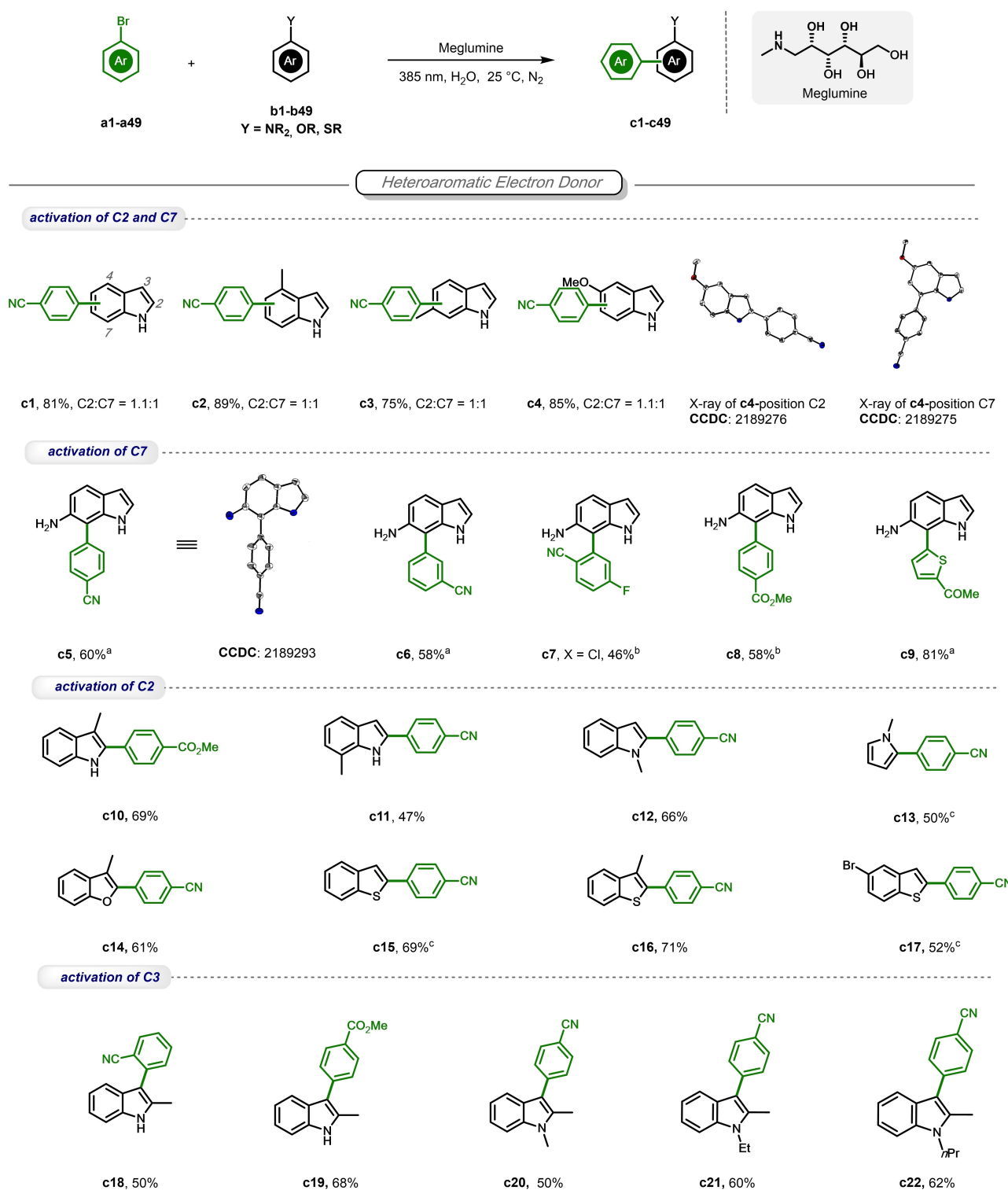


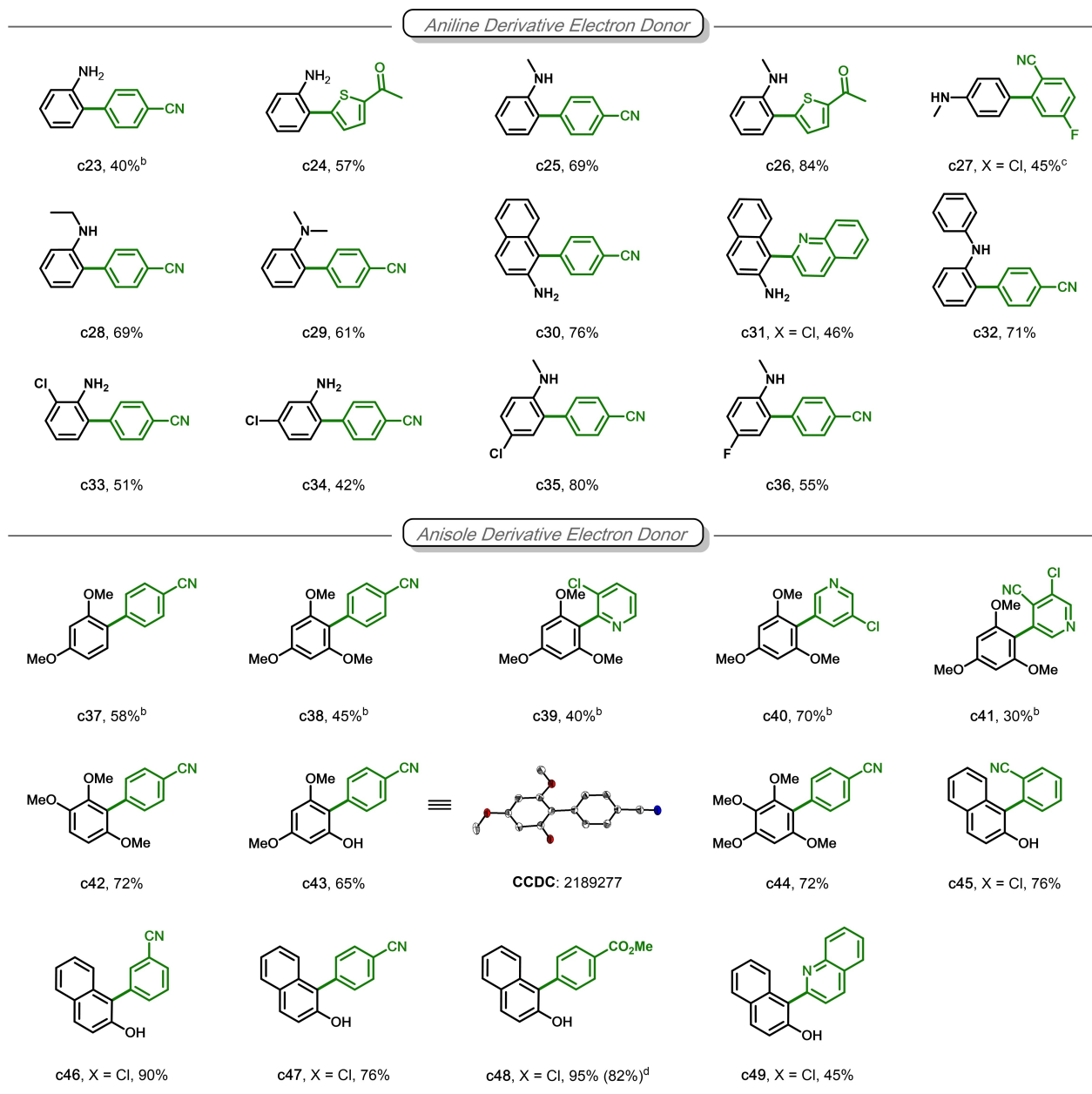
**Figure 1.** Photochemical cross-coupling reactions in water.



**Scheme 1.** Substrate scope of C–C cross-coupling monoarylation reactions. Reaction conditions: **a1–a49** (0.5 mmol), **b1–b49** (0.75 mmol) and meglumine (1.25 mmol) in 6 mL H<sub>2</sub>O under 385 nm LED (2.4 W) light irradiation at 25 °C under N<sub>2</sub> atmosphere for 15 h. Reported yields are isolated yields unless stated otherwise. [a] The reaction was conducted at 45 °C. [b] The reaction was conducted at 45 °C for 36 h. [c] Reaction time was 36 h. [d] Isolated yield of gram-scale reaction.

reorganization.<sup>[3,4]</sup> The solvent environment around the amino group may require less change in the solvent reorganization due to hydrogen bonding with water which

can accelerate the subsequent SET process. When indole contains a methyl group at C3, C7 or N1 position (**c10–c12**), the arylation reaction proceeded at C2 position. Similarly,

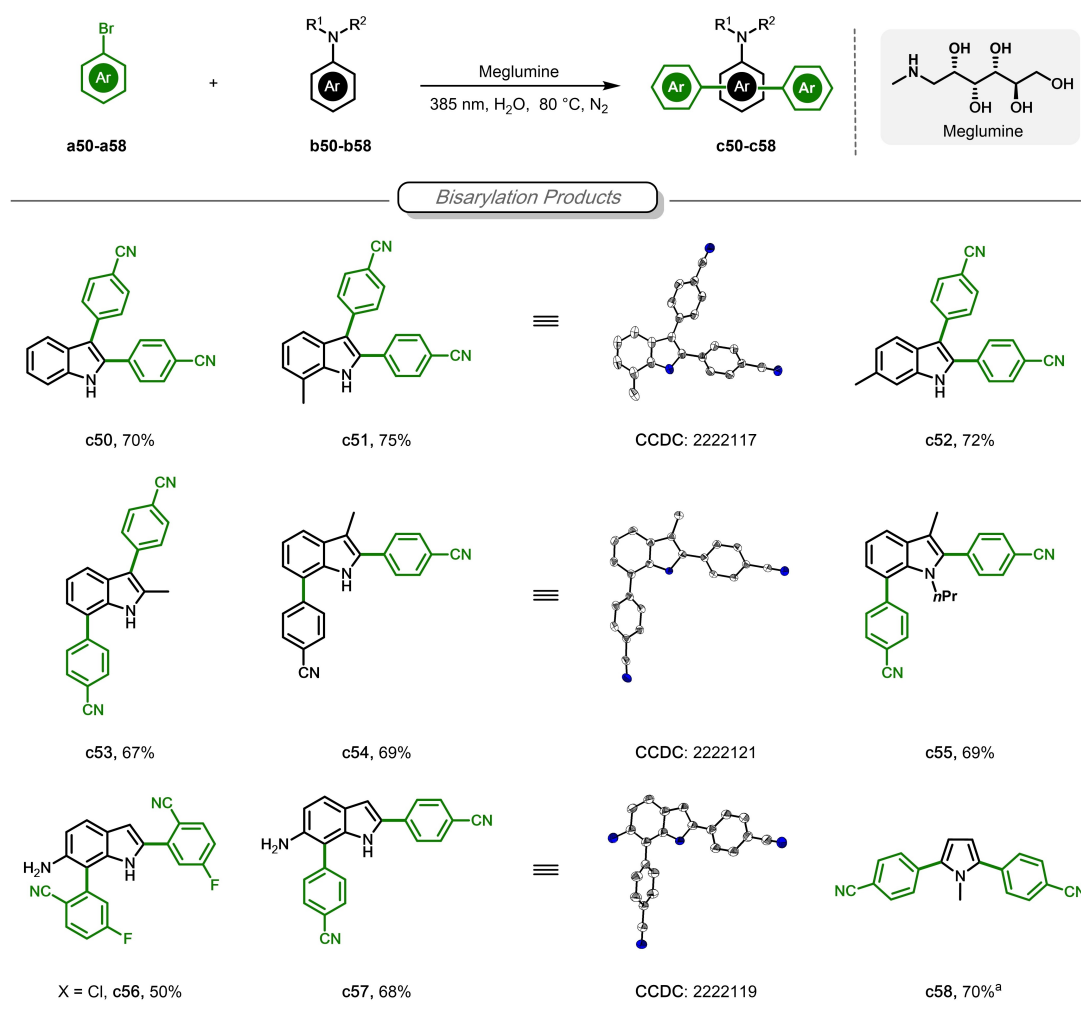


Scheme 2. Continuation of Scheme 1.

N-methylpyrrole (**c13**), 3-methylbenzofuran (**c14**) and benzothiophenes (**c15–c17**) with different functional groups, i.e., CH<sub>3</sub> and Br, also exhibit high selectivity at C2 position. The arylation reaction proceeded at the C3 position of 2-methylindoles (**c18–c22**) due to the increase in the electron cloud density of the pyrrole ring of the indoles. Different electron acceptor substrates (**c6–c10**, **c18**, **c19**) worked well with indoles under the optimized conditions. Aniline (**c23**, **c24**) and derivatives with substituents such as methyl (**c25–c27**, **c29**), ethyl (**c28**), phenyl (**c32**), chlorine (**c33–c35**) and fluorine (**c36**) are also compatible with this standard condition, yielding *ortho*-arylation products. The reactions of 2-aminonaphthalene (**c30**, **c31**) could produce 1-arylation products with high selectivity and good yields. Furthermore,

this method was successfully extended to anisole derivatives (**c37–c44**). Similarly, the reactions of 2-hydroxynaphthalene (**c45–c49**) could provide 1-arylation products with high selectivity. The reaction of **a48** was also conducted in gram scale under optimized conditions, giving 82 % yield of product **c48**. The structures of products **c4-2**, **c4-7**, **c5**, **c43** were confirmed by single-crystal X-ray diffraction.

We then explored the scope under standard conditions for bis-arylation reactions (Scheme 3). Indole (**c50**), 7-methylindole (**c51**) and 6-methylindole (**c52**) yielded the bis-arylation products at C2 and C3 positions. When the C2 or C3 position of indole is substituted by methyl group, the reactions proceeded at C3, C7 (**c53**) and C2, C7 (**c54**, **c55**) positions, respectively. The reactive sites of 6-aminoindole



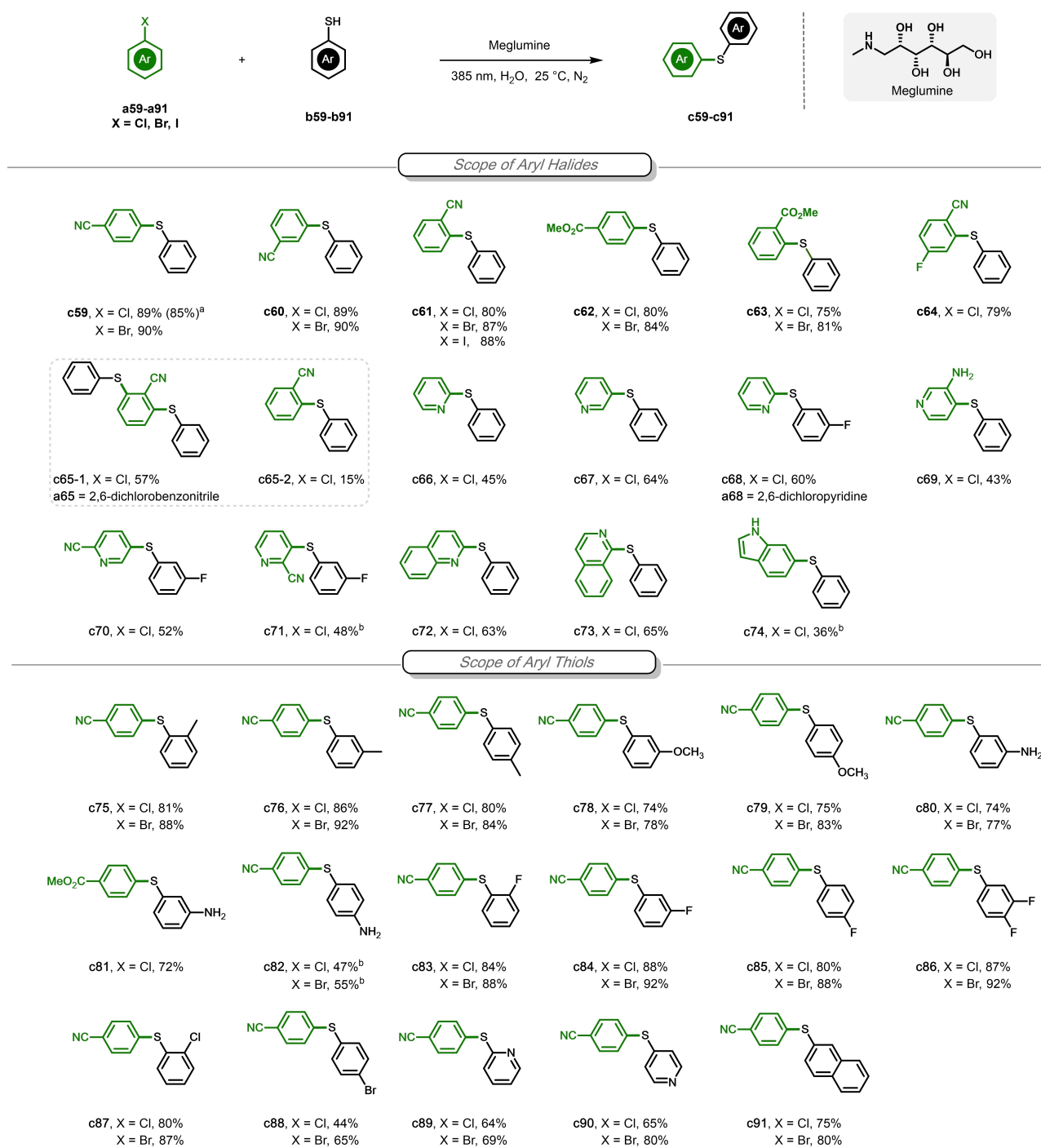
**Scheme 3.** Substrate scope of C–C cross-coupling bis-arylation reactions. Reaction conditions: **a50–a58** (2 mmol), **b50–b58** (0.5 mmol) and meglumine (2 mmol) in 6 mL H<sub>2</sub>O under 385 nm LED (2.4 W) light irradiation at 80 °C under N<sub>2</sub> atmosphere for 15 h. Reported yields are isolated yields unless stated otherwise. [a] The reaction was conducted at 35 °C.

were C2 and C7, which is probably due to the sequential reaction process of this system. Deduced from the mono-arylation of 6-aminoindole (**c5–c9**), the reaction started with the activation of C7, followed by the reaction of C2 position. This condition tolerated the bis-arylation of N-methylpyrrole (**c58**) at C2 position.

After exploration of the photochemical sp<sup>2</sup>–sp<sup>2</sup> C–C cross-coupling in water, we investigated sp<sup>2</sup> C–S coupling reactions employing 4-chlorobenzonitrile (**a59**) and benzenethiol (**b59**) as model substrates. After optimizing the reaction conditions (Tables S7–S11), we obtained the desired product **c59** in 91 % yield using water as solvent in the presence of meglumine under 385 nm light irradiation at 25 °C for 15 h. Control experiments proved that this reaction is a photochemical reaction (Table S7). No product was detected in the absence of meglumine (Table S7, entry 4), indicating that meglumine is indispensable for this transformation. The reaction proceeds as well in DMF but produced much more dechlorinated product than in water (Table S7, entry 6), proving the pivotal role of water for this

reaction. We further evaluated the scope of the reaction under standard conditions (Scheme 4). Halobenzenes with different substituents such as CN (**c59–c61**), CO<sub>2</sub>CH<sub>3</sub> (**c62**, **c63**), and F (**c64**) reacted smoothly to afford the corresponding C–S coupling products in good to excellent yields. 2,6-dichlorobenzonitrile yielded both di-arylation (**c65-1**) and mono-arylation (**c65-2**) products. In addition, this approach was successfully extended to heteroaryl chlorides, such as chloropyridines (**c66–c71**), chloroquinolines (**c72**, **c73**) and chlorindole (**c74**). Furthermore, both electron-rich, with CH<sub>3</sub> (**c75–c77**), OCH<sub>3</sub> (**c78**, **c79**) and NH<sub>2</sub> (**c80–c82**) groups, and electron-deficient, with F (**c83–c86**), Cl (**c87**) and Br (**c88**) groups, benzenethiols were well tolerated. Pyridinethiols (**c89**, **c90**) and 2-naphthalenethiol (**c91**) are also compatible substrates. The reaction of **a59** with **b59** was also conducted in gram scale under optimized conditions, giving 85 % yield of product **c59**.

When 4-bromobenzonitrile (**a1**) and indole (**b1**) were combined for C–C coupling in the absence of meglumine in water, the solution gradually turned cloudy opaque (Fig-



**Scheme 4.** Substrate scope of C–S cross-coupling reactions. Reaction conditions: **a59–a91** (0.5 mmol), **b59–b91** (0.75 mmol) and meglumine (1.25 mmol) in 6 mL H<sub>2</sub>O under 385 nm LED (0.7 W) light irradiation at 25 °C under N<sub>2</sub> atmosphere for 15 h. Reported yields are isolated yields unless stated otherwise. [a] Isolated yield of gram-scale reaction. [b] Reaction time was 48 h.

ure S1). To provide insight into the mechanism of photo-induced C–C and C–S cross-coupling reactions in water, a series of spectroscopic experiments was conducted. First, UV/Vis spectra of different reagent combinations were recorded. The mixture of **a1** and **b1** (Figure 2a, orange line) displays a new absorption band in the visible region. The absorption intensity of the solution with meglumine is

significantly higher than that without meglumine (Figure 2a, purple line) due to its solubilizing effect for the organic aromatic molecules. The absorption spectra were monitored over time and show a gradual increase in absorption intensity over time in the presence of meglumine (Figure 2b), it remained constant over the same time period without meglumine (Figure 2c).

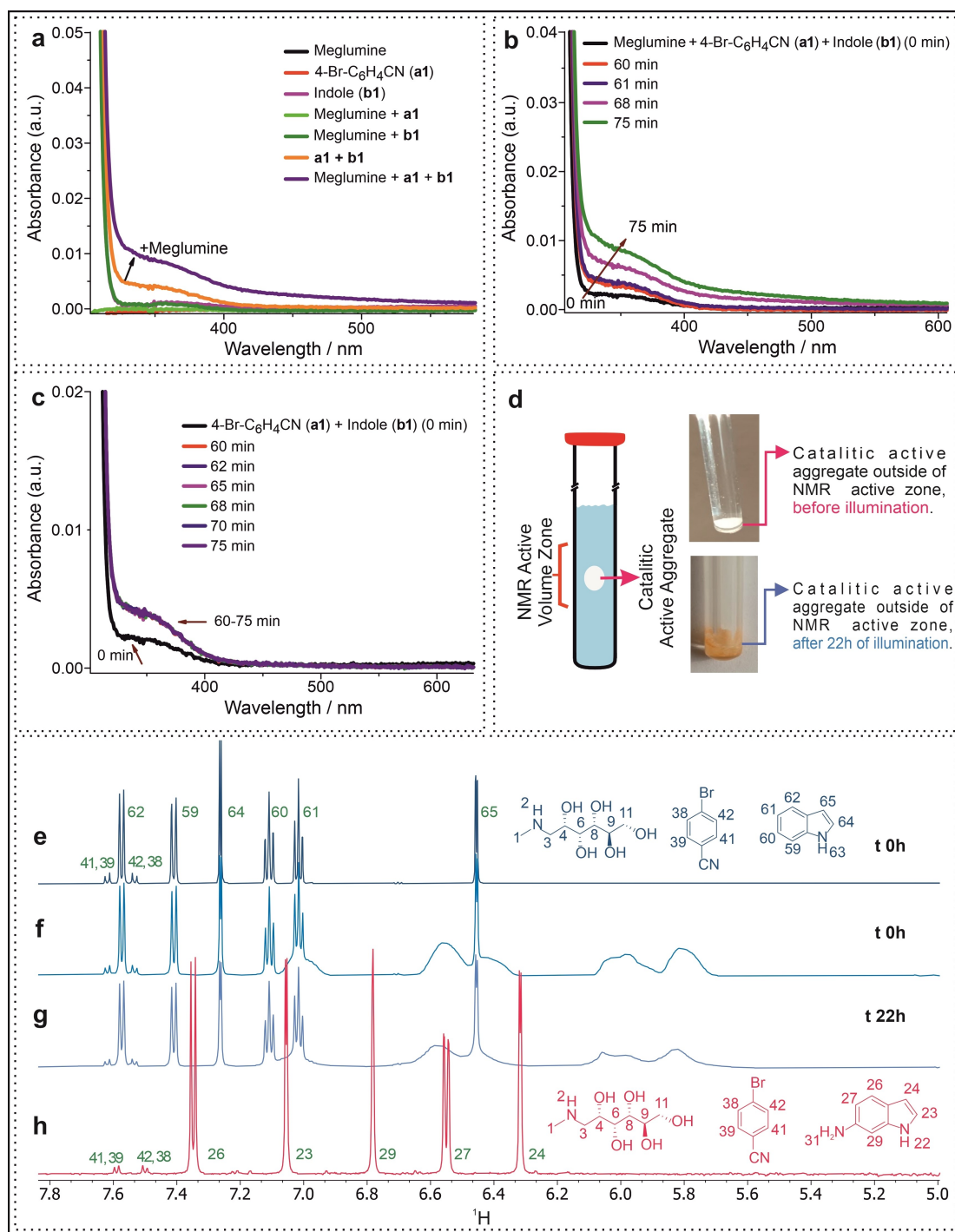


**Figure 2.** Measurements to investigate the mechanism of C–C coupling reaction. **a**) UV/Vis absorption spectra of mixtures **a1**, **b1** and meglumine in water show that meglumine enhances the solubility of the EDA complex in water. The black line (Meglumine) in the spectrum is not visible because it does not absorb at all in this wavelength range and overlaps the baseline. The red line (4-Br-C<sub>6</sub>H<sub>4</sub>CN, **a1**) overlaps the green line (Meglumine + **a1**). The pink purple line (Indole, **b1**) overlaps the dark green line (Meglumine + **b1**). **b**) With meglumine, the UV/Vis absorption spectra of mixture of **a1** and **b1** show a gradual increase in absorption intensity in water over time. **c**) Without meglumine, the UV/Vis absorption spectra of mixture of **a1** and **b1** show constant absorption intensity in water over the same time period. **d**) Schematic diagram of the NMR active volume zone (left) and comparison pictures of the mixture of 0.05 M 4-bromobenzonitrile (**a1**) + 0.07 M indole (**b1**) + 0.125 M meglumine in D<sub>2</sub>O before (top right) and after illumination (bottom right) out of the NMR detection zone. **e**) <sup>1</sup>H spectrum of mixture of 0.05 M 4-bromobenzonitrile (**a1**) + 0.07 M indole (**b1**) + 0.125 M meglumine in D<sub>2</sub>O with the aggregate capsule out of the NMR detection zone. **f**) With the aggregate capsule inside of NMR detection zone before illumination. **g**) With the aggregate capsule inside of the NMR detection zone after 22 h of illumination. **h**) In contrast, the <sup>1</sup>H spectrum of 0.05 M 4-bromobenzonitrile (**a1**) + 0.075 M 6-aminoindole (**b13**) + 0.1 M meglumine in D<sub>2</sub>O does not show aggregation.

In situ NMR studies of a mixture of 4-bromobenzonitrile (**a1**), indole (**b1**) and meglumine in D<sub>2</sub>O were conducted to reveal interaction patterns between the reactants (Figures S5–S13). Without light a spherical capsule forms at the bottom of the NMR-tube, which represents the active zone for catalysis as seen by the color change in Figure 2d and corroborated by several NMR experiments. By forcing this capsule into the active zone of the NMR coils several broad resonance peaks could be detected (Figures 2f and 2g). These broad signals appear only in mixtures of all three components, show <sup>1</sup>H/<sup>13</sup>C combinations typical for aromatic systems and are high field shifted compared to the signals of **a1** or **b1**. The absence of peaks in NOESY spectra indicated that meglumine did not form a tight complex with **a1** or **b1**. Exclusively, the broad signals show intensive NOEs with all protons of meglumine (Figure S12). Thus, only aggregates composed of both **a1** and **b1** are able to interact with meglumine, with the high field shift suggesting a  $\pi/\pi$  stacking. The  $\pi/\pi$  stacking of **a1** and **b1** is also corroborated by an intermolecular contact in a 2D NOESY spectrum of the two substances alone (Figure S10). Taken together, **a1**, **b1** and meglumine form in a synergetic way a special phase

allowing for an effective but unselective catalysis within aggregates.

In contrast, for the highly selective transformation of 6-aminoindole (**b5**) with 4-bromobenzonitrile (**a1**) in the presence of meglumine, a clear homogeneous solution and exclusively sharp signals were observed (Figure 2h). In addition, selective 1D-NOE experiments showed weak interactions between **b5** and meglumine (Figures S14–S18). The comparison between **b1** and **b5** seems to indicate that a reduced aggregation and as a result a smaller conformational or structural space is beneficial for the selectivity of the catalysis.

When 4-methylbenzenethiol (**b77**) and meglumine were mixed for C–S coupling in water, the solution became turbid (Figure S2), and the absorption spectrum is bathochromically shifted (Figure 3a), indicating an interaction between **b77** and meglumine, which likely corresponds to the partial formation of the thiophenolate anion. No change of the UV/Vis spectrum was observed when **a1** and **b77** were mixed (Figure 3a).

In the NMR spectra (Figures 4a, 4b and S19), three sets of signals are observed for 4-methylbenzenethiol (labeled as

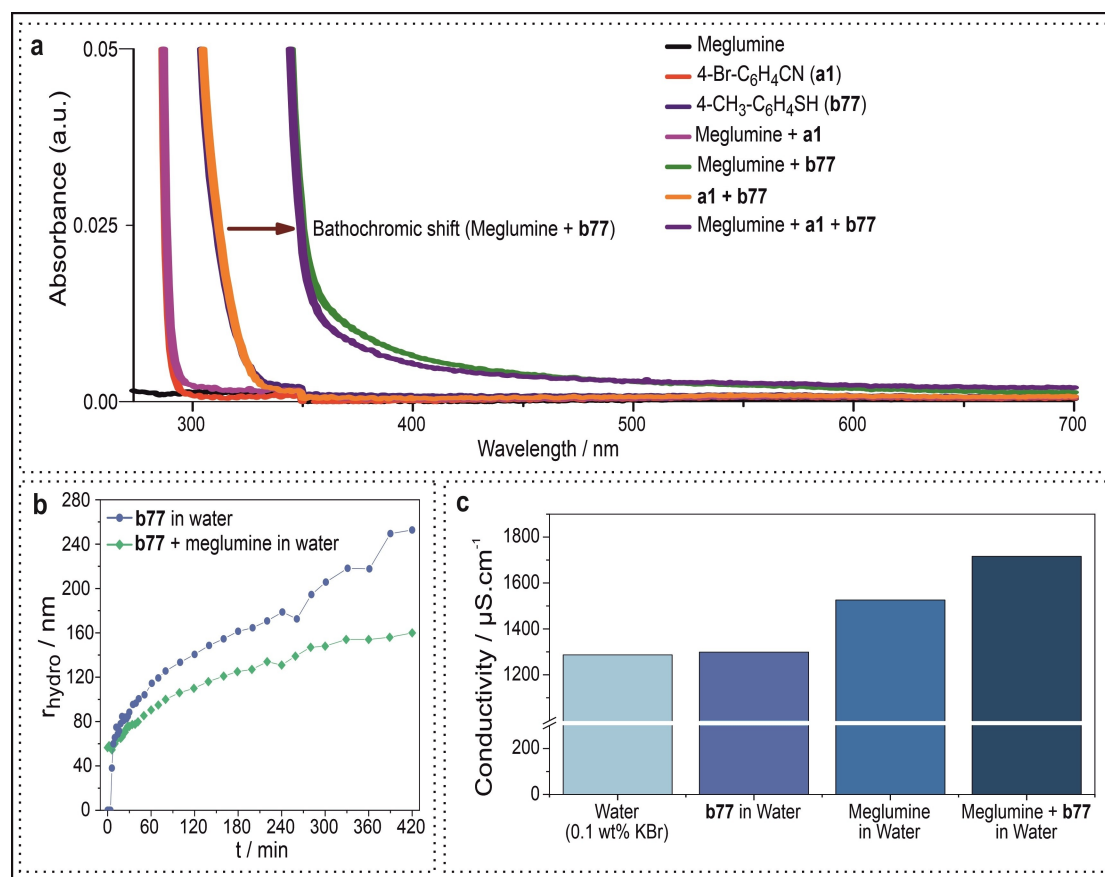


**Figure 3.** Measurements to investigate the mechanism of C–S coupling reaction. **a**) Comparison of the UV/Vis absorption spectra of mixtures of 4-bromobenzonitrile (**a1**), 4-methylbenzenethiol (**b77**) and meglumine in water. **b**) Hydrodynamic radii as a function of time in aqueous solutions containing **b77** with (green curve) and without (blue curve) meglumine determined by DLS measurements at 25 °C show a constant grow of microcrystals over time, which is reduced by meglumine. **c**) Conductivity measurements of aqueous solutions at 25 °C reveal the deprotonation reaction between 4-methylbenzenethiol (**b77a**) and meglumine, confirming that the most abundant species **b77a** is the reactive species rather than the microcrystalline like substrate **b77b**. The solutions contain 0.05 mol/L meglumine, 0.02 mol/L **b77**, and both or none of the additives.

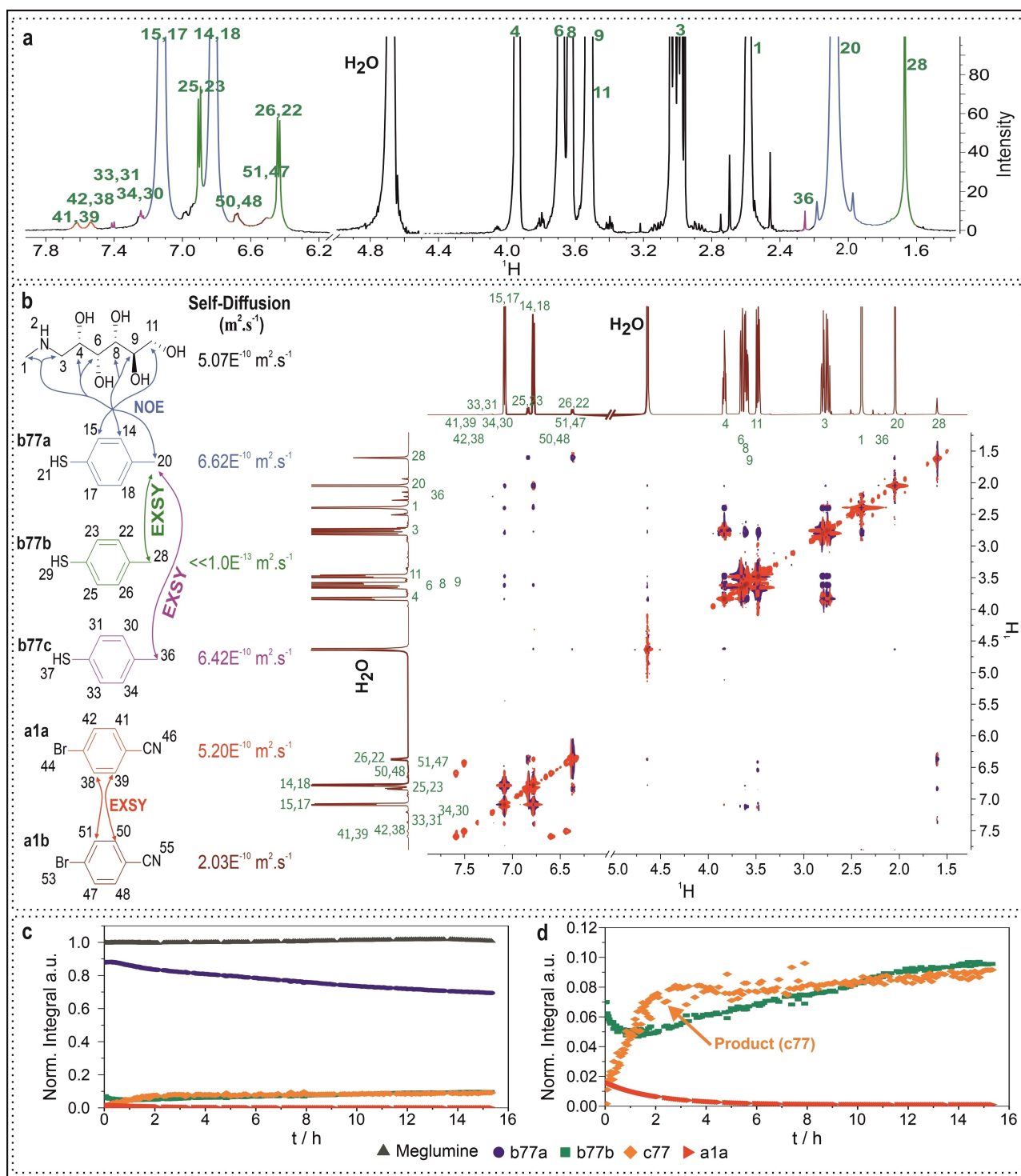


**Figure 4.** Measurements to investigate the mechanism of C–S coupling reaction. **a**)  $^1\text{H}$  spectrum of **a1** (0.05 mmol) and **b77** (0.075 mmol) in the presence of meglumine (0.125 mmol) in  $\text{D}_2\text{O}$  (1 mL). **b**) NMR spectra of **a1** (0.05 mmol) and **b77** (0.075 mmol) in the presence of meglumine (0.125 mmol) in  $\text{D}_2\text{O}$  (1 mL) show several sets of signals for both **a1** and **b77**, their NOE, exchange interactions and self-diffusion coefficients show unspecific interactions, micro crystals and three compartments (for details see text and Figures S21–S24). **c**) In situ NMR reaction profile of the reaction of **a1** (0.05 mmol) and **b77** (0.075 mmol) in the presence of meglumine (0.125 mmol) in  $\text{D}_2\text{O}$  (1 mL) without stirring and under illumination (365 nm). **d**) Expanded region to show the development of **b77b** versus the product **c77**. The minimum of **b77b** in combination with an initially stable concentration of **b77a** suggest a “stock function” of **b77b** (for details see text).

**b77a**, **b77b**, and **b77c** in Figure 4b; relative integrals, meglumine: **b77a**:**b77b**:**b77c**=100:52:11:0.4) for a mixture

of **b77** and meglumine. These three 4-methylbenzenethiol sets are in slow exchange on the NMR time scale as

evidenced by exchange cross peaks (EXSY) (Figures 4b and S21–S24). NOESY spectra showed contacts to meglumine exclusively for the most abundant species **b77a** (Figures 4b and S21–S24) indicating a rather unspecific orientation. The substrate **b77b** diffused much slower than the other substrates with a diffusion coefficient being smaller than  $1 \text{ E}^{-13} \text{ m}^2 \text{ s}^{-1}$ . The combination of small linewidths and extremely low diffusion coefficient hints at a microcrystal structure as discussed below in the light scattering section. The low populated third specie **b77c**, has a similar diffusion coefficient as **b77a** but the low concentration prevented any additional investigations of the structure (Figure 4b). For bromobenzonitrile, two sets of signals were detected showing exchange peaks in the NOESY spectrum (Figure 4b-a1a and 4b-a1b). The diffusion coefficients of these species are slightly different indicating that we have different compartments in the reaction mixture.

Next, we studied the kinetics of the photochemical reaction of 4-bromobenzonitrile (**a1**) with 4-methylbenzenethiol (**b77**) in the presence of meglumine by in situ NMR (Figures 4c and 4d). The product formation (**c77**, orange curve in Figure 4d) started without any delay and also the dissolved **a1a** was completely consumed in 6 hours without further replenishment due to lack of stirring in the NMR tube. Interestingly, the substrate **b77a** stabilized by meglumine remains constant for nearly 1 h and is only afterwards continuously consumed to produce **c77**. Instead of **b77a**, the microcrystalline like substrate **b77b** was consumed from the beginning most probably feeding 4-methylbenzenethiol via the meglumine/**b77a** complex into the reaction. After 80 minutes of the photochemical reaction, the concentration of **b77b** reached a minimum and increased again. This agrees with the existence of microcrystals shown via dynamic light scattering (DLS) and polarization microscope measurements (Figures 3b and S29) and discussed below. The minimum of **b77b** suggests that first **b77b** microcrystals feed the 4-methylbenzenethiol/meglumine complex **b77a**, which is supposed to be the reactive species (constant region of **b77a**, decrease of **b77b**). Then the constant crystal growth from **b77b** takes over and the meglumine/**b77a** complex is consumed for further reaction.

DLS measurements of 4-methylbenzenethiol (**b77**) in water showed aggregation signals after several minutes (Figure 3b), representing fast-growing aggregates that originate from the crystal growth of the substrate itself. DLS analysis of a mixture of **b77** and meglumine in water revealed that meglumine reduced the aggregation (Figure 3b), confirming the interaction between **b77** and meglumine. Subsequent polarization microscope measurements (Figure S29) of **b77** in water confirmed this hypothesis. Crystals were obtained immediately after filtration, indicating rapid precipitation of **b77** albeit slower than without meglumine. Therefore, the subsequent increase in **b77b** concentration (Figure 4d-b77b) was due to the crystal growth of the substrate itself. Even after total consumption of **a1** in the liquid phase, **b77a** continued to decrease followed by a subtle increase in **b77b** (Figures 4c and 4d), suggesting that **b77b** functions as a “stock” of this substrate

and is related to the growth of aggregates and crystals. How **b77c** participated in this reaction is not clear, its diffusion coefficient showed that this substrate was in a different domain than its homonyms, having faster diffusion than **b77b** and slightly slower diffusion than **b77a** (Figure 4b). This could be a linking domain between the **b77a** and **b77b**. The final product was mainly formed in the first 2 h due to the lack of mixing in the NMR tube and meglumine concentration remained constant during the reaction (Figures 4c and 4d).

Conductivity measurements (Figures 3c and S31) demonstrated that basic meglumine increases conductivity in aqueous solution and the conductivity of such meglumine aqueous solution further increases by adding 4-methylbenzenethiol, indicating that an acid-base reaction deprotonating 4-methylbenzenethiol (Figure S31) occurs between 4-methylbenzenethiol (**b77a**) and meglumine, leading to a higher amount of charge carrier and thus higher conductivity. In addition, combined with the NMR results (Figure 4b), the conductivity investigations further confirm that the soluble **b77a** is the reactive species rather than the microcrystalline **b77b**.

Considering these observations, mechanisms for the photo-induced C–C and C–S cross-coupling reactions in water are proposed (Figure 5). For the C–C coupling, the electron acceptor molecule and the electron donor molecule aggregate in the ground state forming an EDA complex. Meglumine significantly enhances the solubility of the EDA complex in water. Meglumine as a basic compound also acts as a base in the reaction. 385 nm light irradiation excites the EDA complex and triggers a single electron transfer (SET) process to produce a radical ion pair. The radical anion eliminates a halide anion resulting in a neutral arene radical. These two radical intermediates couple to give the final product. In the C–S coupling system, one molecule of meglumine aggregates with three molecules of arylthiol in water. Partial deprotonation of the **b77a** arylthiol substrate by meglumine leads to a thiolate anion, which further associates with aryl halide, generating an EDA complex. The other two arylthiols (**b77b** and **b77c**) in turn supply the consumption of the **b77a**. Similar to the C–C coupling, the excess meglumine enhances the solubility of the EDA complex in water. Light excitation triggers charge transfer between the thiolate anion and aryl halide to generate thiyl radical and aryl radical, which subsequently produce the desired arylthiolation coupling product. Maybe, there are other subtle interactions, e.g., of meglumine with the excited state or the products that further favour the reactions and trigger the bond specificities. It is well-known that additives like meglumine with sugar moieties can have various effects and play the role as osmolytes, hydrotropes, co-solutes etc. inducing depletion effects, salting-in and salting-out, stabilizing selectively aggregates, transition states etc.<sup>[48,49]</sup> However, without detailed simulations efforts, we cannot conclude in more details about the role of meglumine in the present systems.

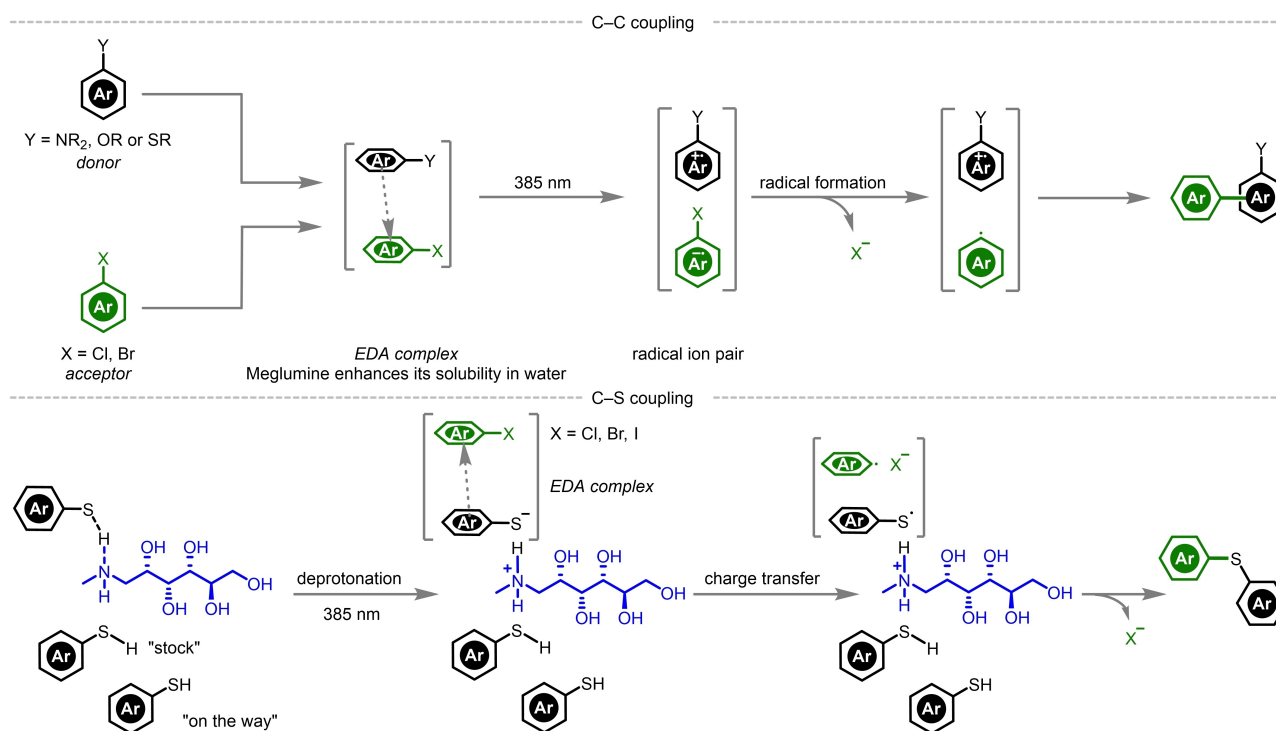


Figure 5. Proposed reaction mechanisms.

## Conclusion

In conclusion, we have developed a metal- and photoredox catalyst-free room temperature photochemical arylation and arylthiolation of (hetero)aryl halides by using water as reaction medium. Meglumine serves as additive for the photochemical transformations in water to enhance the solubility of the organic components. Moreover, meglumine binds and deprotonates arylthiols giving thiolate anions, which then form EDA complexes with aryl halides. The orientation of the reactants in EDA complexes in water allows the C–H arylation of indoles at their carbocyclic ring without protecting the N–H group, which, to the best of our knowledge, cannot be directly achieved otherwise. The easy to execute protocol with good functional group compatibility and broad scope illustrates the potential of enforced aggregate formation in water for photochemical transformations in organic synthesis.

## Acknowledgements

This work was supported by the Deutsche Forschungsgemeinschaft (DFG, German Science Foundation)—TRR 325—444632635. Y.-M. Tian thanks Yijia Zhao (University of Southampton) for her assistance in producing the Figures in the manuscript. E. Hofmann thanks the Fonds der Chemischen Industrie (FCI) for her scholarship. Wagner Silva is funded by Deutsche Forschungsgemeinschaft (RTG 2620 Ion Pair Effects in Molecular Reactivity, Project 426795949). We thank Dr. Rudolf Vasold (University of Regensburg)

for his assistance in GC-MS measurements and Birgit Hischa (University of Regensburg) for her assistance in single crystal X-ray measurements. Open Access funding enabled and organized by Projekt DEAL.

## Conflict of Interest

The authors declare no conflict of interest.

## Data Availability Statement

The data that support the findings of this study are available from the corresponding author upon reasonable request.

**Keywords:** Arylation • EDA Complex • Meglumine • Photochemistry • Water

- [1] R. Foster, *J. Phys. Chem.* **1980**, *84*, 2135–2141.
- [2] S. V. Rosokha, J. K. Kochi, *Acc. Chem. Res.* **2008**, *41*, 641–653.
- [3] T. Mori, Y. Inoue, *Chem. Soc. Rev.* **2013**, *42*, 8122–8133.
- [4] C. G. S. Lima, T. d M Lima, M. Duarte, I. D. Jurberg, M. W. Paixão, *ACS Catal.* **2016**, *6*, 1389–1407.
- [5] G. E. M. Crisenza, D. Mazzarella, P. Melchiorre, *J. Am. Chem. Soc.* **2020**, *142*, 5461–5476.
- [6] R. S. Mulliken, *J. Am. Chem. Soc.* **1950**, *72*, 600–608.
- [7] R. S. Mulliken, *J. Am. Chem. Soc.* **1952**, *74*, 811–824.
- [8] R. S. Mulliken, *J. Phys. Chem.* **1952**, *56*, 801–822.
- [9] J. Anunziata, J. Singh, J. J. Silber, *Can. J. Chem.* **1981**, *59*, 1291–1296.

- [10] E. F. Hilinski, J. M. Masnovi, C. Amatore, J. K. Kochi, P. M. Rentzepis, *J. Am. Chem. Soc.* **1983**, *105*, 6167–6168.
- [11] D. Cantacuzène, C. Wakselman, R. Dorme, *J. Chem. Soc. Perkin Trans. 1* **1977**, 1365–1371.
- [12] J. F. Bunnett, *Acc. Chem. Res.* **1978**, *11*, 413–420.
- [13] S. Fukuzumi, K. Mochida, J. K. Kochi, *J. Am. Chem. Soc.* **1979**, *101*, 5961–5972.
- [14] M. A. Fox, J. Younathan, G. E. Fryxell, *J. Org. Chem.* **1983**, *48*, 3109–3112.
- [15] P. A. Wade, H. A. Morrison, N. Kornblum, *J. Org. Chem.* **1987**, *52*, 3102–3107.
- [16] S. Sankararaman, W. A. Haney, J. K. Kochi, *J. Am. Chem. Soc.* **1987**, *109*, 7824–7838.
- [17] G. A. Russell, K. Wang, *J. Org. Chem.* **1991**, *56*, 3475–3479.
- [18] T. Gotoh, A. B. Padias, J. H. K. Hall, *J. Am. Chem. Soc.* **1991**, *113*, 1308–1312.
- [19] M. Tobisu, T. Furukawa, N. Chatani, *Chem. Lett.* **2013**, *42*, 1203–1205.
- [20] E. Arceo, I. D. Jurberg, A. Álvarez-Fernández, P. Melchiorre, *Nat. Chem.* **2013**, *5*, 750–756.
- [21] I. Bosque, T. Bach, *ACS Catal.* **2019**, *9*, 9103–9109.
- [22] S. R. Kandukuri, A. Bahamonde, I. Chatterjee, I. D. Jurberg, E. C. Escudero-Adán, P. Melchiorre, *Angew. Chem. Int. Ed.* **2015**, *54*, 1485–1489; *Angew. Chem.* **2015**, *127*, 1505–1509.
- [23] L. Marzo, S. Wang, B. König, *Org. Lett.* **2017**, *19*, 5976–5979.
- [24] Z. Yang, Y. Liu, K. Cao, X. Zhang, H. Jiang, J. Li, *Beilstein J. Org. Chem.* **2021**, *17*, 771–799.
- [25] Y. Wei, Q.-Q. Zhou, F. Tan, L.-Q. Lu, W.-J. Xiao, *Synthesis* **2019**, *51*, 3021–3054.
- [26] M. J. James, F. Strieth-Kalthoff, F. Sandfort, F. J. R. Klauck, F. Wagener, F. Glorius, *Chem. Eur. J.* **2019**, *25*, 8240–8244.
- [27] B. Liu, C.-H. Lim, G. M. Miyake, *J. Am. Chem. Soc.* **2017**, *139*, 13616–13619.
- [28] M. J. Cabrera-Afonso, A. Granados, G. A. Molander, *Angew. Chem. Int. Ed.* **2022**, *61*, e202202706; *Angew. Chem.* **2022**, *134*, e202202706.
- [29] A. Wimmer, B. König, *Beilstein J. Org. Chem.* **2018**, *14*, 54–83.
- [30] S. Xie, D. Li, H. Huang, F. Zhang, Y. Chen, *J. Am. Chem. Soc.* **2019**, *141*, 16237–16242.
- [31] M. Nappi, G. Bergonzini, P. Melchiorre, *Angew. Chem. Int. Ed.* **2014**, *53*, 4921–4925; *Angew. Chem.* **2014**, *126*, 5021–5025.
- [32] K. Liang, N. Li, Y. Zhang, T. Li, C. Xia, *Chem. Sci.* **2019**, *10*, 3049–3053.
- [33] Y. Wang, J. Wang, G.-X. Li, G. He, G. Chen, *Org. Lett.* **2017**, *19*, 1442–1445.
- [34] A. Fawcett, J. Pradeilles, Y. Wang, T. Mutsuga, E. L. Myers, V. K. Aggarwal, *Science* **2017**, *357*, 283–286.
- [35] F. Sandfort, F. Strieth-Kalthoff, F. J. R. Klauck, M. J. James, F. Glorius, *Chem. Eur. J.* **2018**, *24*, 17210–17214.
- [36] M. H. Aukland, M. Šiaučius, A. West, G. J. P. Perry, D. J. Procter, *Nat. Catal.* **2020**, *3*, 163–169.
- [37] C. K. Prier, F. H. Arnold, *J. Am. Chem. Soc.* **2015**, *137*, 13992–14006.
- [38] M. A. Emmanuel, N. R. Greenberg, D. G. Oblinsky, T. K. Hyster, *Nature* **2016**, *540*, 414–417.
- [39] K. F. Biegasiewicz, S. J. Cooper, X. Gao, D. G. Oblinsky, J. H. Kim, S. E. Garfinkle, L. A. Joyce, B. A. Sandoval, G. D. Scholes, T. K. Hyster, *Science* **2019**, *364*, 1166–1169.
- [40] C. Aloisio, A. G. de Oliveira, M. Longhi, *J. Pharm. Sci.* **2016**, *105*, 2703–2711.
- [41] G. Sravya, G. Suresh, G. V. Zyryanov, A. Balakrishna, K. M. K. Reddy, C. S. Reddy, C. Venkataramaiah, W. Rajendra, N. B. Reddy, *J. Heterocycl. Chem.* **2020**, *57*, 355–369.
- [42] C. Aloisio, M. R. Longhi, A. G. De Oliveira, *J. Pharm. Sci.* **2015**, *104*, 3535–3543.
- [43] C. Aloisio, A. G. de Oliveira, M. Longhi, *J. Pharm. Biomed. Anal.* **2014**, *100*, 64–73.
- [44] C. Aloisio, A. G. de Oliveira, M. Longhi, *Drug Dev. Ind. Pharm.* **2014**, *40*, 919–928.
- [45] P. Gupta, A. K. Bansal, *Pharmazie* **2005**, *60*, 830–836.
- [46] F. Frézard, P. S. Martins, A. P. C. O. Bahia, L. L. Moyec, A. L. de Melo, A. M. C. Pimenta, M. Salerno, J. B. B. da Silva, C. Demicheli, *Int. J. Pharm.* **2008**, *347*, 102–108.
- [47] P. Degot, D. Funkner, V. Huber, M. Köglmaier, D. Touraud, W. Kunz, *J. Mol. Liq.* **2021**, *334*, 116478.
- [48] D. Harries, J. Rösger, *Methods Cell Biol.* **2008**, *84*, 679–735.
- [49] I. Shumilin, C. Alolio, D. Harries, *J. Am. Chem. Soc.* **2019**, *141*, 18056–18063.
- [50] Deposition numbers 2189272 (**c1-7**), 2189276 (**c4-2**), 2189275 (**c4-7**), 2189293 (**c5**), 2189277 (**c43**), 2222117 (**c51**), 2222121 (**c54**), 2222119 (**c57**) contain the supplementary crystallographic data for this paper. These data are provided free of charge by the joint Cambridge Crystallographic Data Centre and Fachinformationszentrum Karlsruhe Access Structures service.

Manuscript received: December 19, 2022

Accepted manuscript online: February 3, 2023

Version of record online: March 8, 2023